

New Galactic Star Clusters Discovered in the VVV Survey*

J. Borissova¹, C. Bonatto², R. Kurtev¹, J. R. A. Clarke¹, F. Peñaloza¹, S. E. Sale^{1,5}, D. Minniti^{5,17}, J. Alonso-García⁵, E. Artigau³, R. Barbá¹⁶, E. Bica², G. L. Baume⁴, M. Catelan⁵, A. N. Chenè^{1,6}, B. Dias⁷, S. L. Folkes¹, D. Froebrich⁸, D. Geisler⁶, R. de Grijs^{9,10}, M. M. Hanson¹⁷, M. Hempel⁵, V. D. Ivanov¹¹, M. S. N. Kumar¹², P. Lucas¹³, F. Mauro⁶, C. Moni Bidin⁶, M. Rejkuba¹⁵, R. K. Saito⁵, M. Tamura¹⁴, and I. Toledo⁵

- ¹ Departamento de Física y Astronomía, Facultad de Ciencias, Universidad de Valparaíso, Av. Gran Bretaña 1111, Playa Ancha, Casilla 5030, Valparaíso, Chile (e-mail: jura.borissova@uv.cl; radostin.kurtev@uv.cl; paco.stilla@gmail.com; j.clarke@dfa.uv.cl; s.folkes@dfa.uv.cl; s.sale@dfa.uv.cl)
- ² Universidade Federal do Rio Grande do Sul, Departamento de Astronomia CP 15051, RS, Porto Alegre 91501-970, Brazil (e-mail: charles@if.ufrgs.br; bica@if.ufrgs.br)
- ³ Département de Physique and Observatoire du Mont Mégantic, Université de Montréal, C.P. 6128, Succ. Centre-Ville, Montréal, QC H3C 3J7, Canada (e-mail: artigau@ASTRO.UMontreal.CA)
- ⁴ Facultad de Ciencias Astronómicas y Geofísicas, Instituto de Astrofísica de La Plata, Paseo del Bosque s/n, La Plata, Argentina (e-mail: gbaume@gmail.com)
- ⁵ Departamento de Astronomía y Astrofísica, Pontificia Universidad Católica de Chile, Av. Vicuña Mackenna 4860, Casilla 306, Santiago 22, Chile (e-mail: dante@astro.puc.cl; mcatean@astro.puc.cl; itoledoc@gmail.com; mhempel@astro.puc.cl; rsaito@astro.puc.cl; jalonso@astro.puc.cl)
- ⁶ Departamento de Astronomía, Casilla 160, Universidad de Concepción, Chile (e-mail: achene@udec.cl; dgeisler@astro-udec.cl)
- ⁷ Departamento de Astronomia, Universidade de Sao Paulo, Rua do Matao, 1226 - Cidade Universitaria, 05508-900 - Sao Paulo/SP - Brasil (e-mail: bdias@astro.iag.usp.br)
- ⁸ Centre for Astrophysics & Planetary Science, The University of Kent, Canterbury, Kent, UK, CT2 7NH (e-mail: df@star.kent.ac.uk)
- ⁹ Kavli Institute for Astronomy and Astrophysics, Peking University, Yi He Yuan Lu 5, Hai Dian District, Beijing 100871, China (e-mail: grijs@pku.edu.cn)
- ¹⁰ Department of Astronomy and Space Science, Kyung Hee University, Yongin-shi, Kyungki-do 449-701, Republic of Korea
- ¹¹ European Southern Observatory, Ave. Alonso de Cordova 3107, Casilla 19, Santiago 19001, Chile (e-mail: vivanov@eso.org)
- ¹² Centro de Astrofísica da Universidade do Porto, Rua das Estrelas, 4150-762 Porto, Portugal (e-mail: nanda@astro.up.pt)
- ¹³ Centre for Astrophysics Research, University of Hertfordshire, Hatfield AL10 9AB, UK (e-mail: phyqpw@herts.ac.uk)
- ¹⁴ National Astronomical Observatory of Japan, Osawa 2-21-1, Mitaka, Tokyo 181-8588, Japan (e-mail: motohide.tamura@nao.ac.jp)
- ¹⁵ European Southern Observatory, Karl-Schwarzschild-Strasse 2, D-85748 Garching bei Munchen, Germany (e-mail: mrejkuba@eso.org)
- ¹⁶ Departamento de Física, Universidad de La Serena, Cisternas 1200 Norte, La Serena, Chile; Instituto de Ciencias Astronómicas, de la Tierra y del Espacio (ICATE-CONICET), Av. España Sur 1512, J5402DSP, San Juan, Argentina (e-mail: rbarba@dfuls.cl)
- ¹⁷ Department of Physics, University of Cincinnati, Cincinnati, OH 45221-0011, USA (e-mail: margaret.hanson@uc.edu)
- ¹⁸ Vatican Observatory, V00120 Vatican City State, Italy

Received; accepted

ABSTRACT

Context. VISTA Variables in the Vía Láctea (VVV) is one of the six ESO Public Surveys operating on the new 4-meter Visible and Infrared Survey Telescope for Astronomy (VISTA). VVV is scanning the Milky Way bulge and an adjacent section of the disk, where star formation activity is high. One of the principal goals of the VVV Survey is to find new star clusters of different ages.

Aims. In order to trace the early epochs of star cluster formation we concentrated our search in the directions to those of known star formation regions, masers, radio, and infrared sources.

Methods. The disk area covered by VVV was visually inspected using the pipeline processed and calibrated K_S -band tile images for stellar overdensities. Subsequently, we examined the composite JHK_S and ZJK_S color images of each candidate. PSF photometry of 15×15 arcmin fields centered on the candidates was then performed on the Cambridge Astronomy Survey Unit reduced images. After statistical field-star decontamination, color-magnitude and color-color diagrams were constructed and analyzed.

Results. We report the discovery of 96 new infrared open clusters and stellar groups. Most of the new cluster candidates are faint and compact (with small angular sizes), highly reddened, and younger than 5 Myr. For relatively well populated cluster candidates we derived their fundamental parameters such as reddening, distance, and age by fitting the solar-metallicity Padova isochrones to the color-magnitude diagrams.

Key words. Galaxy: open clusters and associations; Galaxy: disk; stars: early-type; Infrared: stars.

1. Introduction

It is a well established fact that the majority of stars with masses $>0.50 M_{\odot}$ form in clustered environments (e.g. Lada & Lada 2003, de Wit et al. 2005). Therefore, in understanding the formation, evolution, dynamics, and destruction of star clusters gain insights into the formation, evolution, and dynamics of galaxies. Estimates indicate that the Galaxy presently hosts 35000 or more star clusters (Bonatto et al. 2006, Portegies Zwart et al. 2010). However, only about 2500 open clusters have been identified and constitute a sample affected by several well known selection effects. Less than a half of these clusters have actually been studied, and this subset suffers from further selection biases. Around 1300 clusters, mainly in the infrared have been discovered through automatic or semi-automatic searches of large scale survey data products from DSS, 2MASS, DENIS and GLIMPSE (e.g. Bica et al. 2003, Mercer et al. 2005, Froebrich, Scholz & Raftery 2007, Glushkova et al. 2010). Expectations are that the new generation of all sky surveys (UKIDSS, the VISTA-based VHS and VVV, and Gaia) will add many more. Indeed, a new Galactic globular cluster candidate has been detected already by Minniti et al. (2011) on the initial VVV bulge images.

VVV is one of the six ESO Public Surveys selected to operate with the new 4-meter VISTA telescope (Arnaboldi et al. 2007). VVV is scanning the Milky Way (MW) bulge and an adjacent section of the mid-plane, where star formation activity is high. The survey started in 2010, and it was granted 1929 hours of observing time over a five year period. It covers an area of 520 deg^2 , and is expected to produce a catalog of $\sim 10^9$ point sources (Minniti et al. 2010, Saito et al. 2010). One of the main goals of the VVV Survey is a study of star clusters of different ages in order to build a homogeneous, statistically significant sample in the direction of the Galactic center, thus complementing recent catalogs which are complete up to only 1 kpc from the Sun (version 3.1, 24/nov/2010 of the Dias et al. 2002 catalog; see also Lamers et al. 2005; Piskunov et al. 2008). A sample thus obtained will be used to: 1.) carry out a census of the MW open clusters projected towards the central parts of the Galaxy and in the southern disk covered by VVV; 2.) to establish the contamination by star-cluster like statistical fluctuations in the background and holes in the dust; 3.) to estimate relative cluster formation efficiency in the MW; 4.) to estimate the role of disruption effects; 5.) to put some constraints on the Initial Mass Function; 6.) to compare the Galactic open cluster systems with those of the LMC, SMC, and other extragalactic cluster populations; as well as addressing many other questions. The results presented in this paper are part of a larger program aimed at characterizing the hidden star cluster population in the Galaxy (Borissova et al. 2003, 2005, 2006, 2008, 2009, 2010; Ivanov et al. 2002, 2005, 2010, 2011; Kurtev et al. 2007, 2008, 2009; Hanson et al. 2008, 2010; Bica et al. 2003, Dutra et al. 2003, Longmore et al. 2011). Initially, the project was based on cluster candidates identified from 2MASS (Skrutskie et al. 2006) and the *Spitzer Space Telescope* Galactic Legacy Infrared Mid-Plane Survey Extraordinaire (GLIMPSE, Benjamin et al. 2003) survey. To date we have confirmed three massive star clusters - DBSB 179 (Dutra et al. 2003), Mercer 30 and

Mercer 23 (Mercer et al. 2005) with masses approaching 10^4 solar masses. We also confirmed several new globular clusters (FSR1735, Froebrich et al. 2007; Mercer 3, Kurtev et al. 2008; and Mercer 5, Longmore et al. 2011).

After the first year of the VVV survey we have at our disposal *JHK_S* images of almost the whole disk and bulge area covered by the survey, and *ZY* images for the disk area. In this paper we report the first results of our focused search for new star cluster candidates in the disk area covered by VVV. We concentrated our search towards known star forming regions associated with: methanol maser emission; hot molecular cores (Longmore et al. 2009); galactic bubbles outlined by GLIMPSE (Churchwell et al. 2006, 2007); infrared and radio sources in order to trace the early epochs of star cluster formation.

2. Observations and Data Reduction

The VIRCAM (VISTA Infrared CAMera; Dalton et al. 2006) is a 16 detector-array 1.65 deg^2 infrared camera. Each 2048×2048 detector is sensitive over $\lambda = 0.8 - 2.5 \mu\text{m}$, and it delivers images with an average pixel scale of $0.34 \text{ arcsec px}^{-1}$. A single exposure corresponds to a patchy individual “paw print” coverage on the sky. To fill the gaps, and to obtain a contiguous image, six shifted paw-prints are combined into a “tile” covering 1.5 deg by 1.1 deg , which in the case of VVV, are aligned along Galactic *l* and *b* respectively. The total exposure time of a single tile is 80 sec. To cover the VVV survey area, the disk field is then divided into 152 tiles. The data reduction was carried out in the typical manner for infrared imaging, and details of the procedure are described in Irwin et al. (2004).

3. Cluster Search

Since we were expecting relatively faint and heavily reddened clusters undiscovered in the 2MASS, DENIS, and the GLIMPSE surveys, we first retrieved the pipeline processed and calibrated *ZYJHK_S* tile images from the Cambridge Astronomical Survey Unit (CASU) VIRCAM pipeline v1.0, Irwin et al. 2004) to visually inspected the *K_S*-band tile images for stellar over-densities in the Galactic disk. We then checked the candidates on the composite *JHK_S* and *ZJK_S* color images. Fig. 1 illustrates the process for a typical open cluster candidate, that of VVV CL036. As can be seen, the *Z* and *Y* images do not contain any over-density of stars, while on the *H* and *K_S* images the cluster candidate is obvious. The last image in Fig. 1 shows the composite *ZJK_S* color image of the cluster and the separation between most probable cluster members (red) and field stars (blue). Prior to the use of color-magnitude diagrams our main criterion to define star cluster candidates were a visually compact appearance, distinctive from the surrounding field and with at least 10 stars with similar colors belonging to this cluster candidate.

PSF photometry of 15×15 arcmin fields surrounding each selected candidate was then performed on the CASU reduced images. We used DAOPHOT-II software (Stetson 1987) within the Image Reduction and Analysis Facility (IRAF¹). The PSF was obtained for each frame using approximately a few dozen uncontaminated stars. The typical

Send offprint requests to: J. Borissova

* Based on observations gathered with VIRCAM, VISTA of the ESO as part of observing programs 172.B-2002

¹ IRAF is distributed by the National Optical Astronomy Observatories, which are operated by the Association of

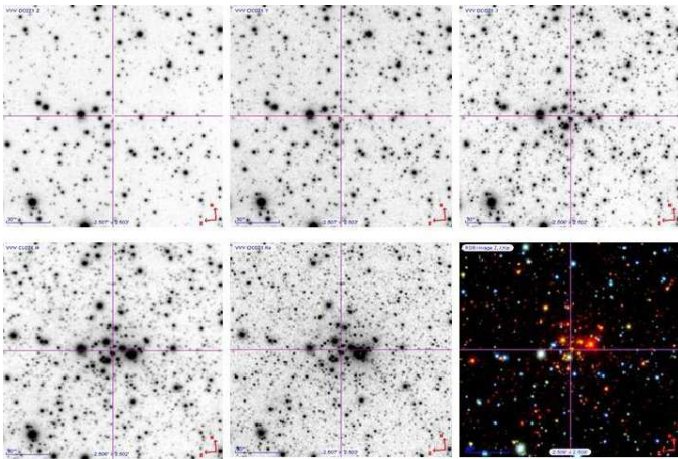


Fig. 1. The VVV $ZYJHK_S$ images and ZJK_S true color image of VVV CL036. The field of view is 2.5×2.5 arcmin, North is up, East to the left.

internal photometric uncertainties vary from 0.005 mag for stars with $K_S \sim 13$ mag to 0.15 mag for $K_S \sim 18$ mag. The J , H and K_S photometry was uniformly calibrated against the 2MASS Point Source Catalog (Skrutskie et al. 2006) generally using several hundred stars in common by least-squares linear regression. For the Z and Y filters we used zero points given in CASU catalogs. Where possible the saturated stars (usually $K_S \leq 13.5$ mag) were replaced by 2MASS point source catalogue stars.

4. Field-star decontamination

In general, poorly-populated clusters, and/or those containing high fractions of faint stars, require field-star decontamination for the identification and characterization of the cluster members. The images of the candidates (Figs. 1 and 4) clearly show that the decontamination is essential to minimize confusion with the red dwarfs of the Galactic field.

For this purpose we used the field-star decontamination algorithm described in Bonatto & Bica (2010, and references therein), adapted to exploit the VVV photometric depth in H and K_S . The first step was to define a comparison field that, depending on the distribution of stars, clusters or extinction clouds in an image, may be the form of a ring around the cluster or other different geometry. The algorithm divides the full range of magnitude and colors of a CMD into a 3D grid of cells with axes along K_S , $(H - K_S)$ and $(J - K_S)$. Initially, cell dimensions were $\Delta K_S = 1.0$ and $\Delta(H - K_S) = \Delta(J - K_S) = 0.2$ mag, but sizes half and twice those values were also used. We also applied shifts in the grid positioning by $\pm 1/3$ of the respective cell size along the 3 axes. Thus, the number of independent decontamination outputs amounted to 729 for each cluster candidate. For each cell, the algorithm estimated the expected number-density of member stars by subtracting the respective field-star number-density². Thus, each grid setup produced a

Universities for Research in Astronomy, Inc., under cooperative agreement with the National Science Foundation

² Photometric uncertainties were taken into account by computing the probability of a star of given magnitude and colors to be found in a any cell (i.e., the difference of the error function computed at the cell's borders).

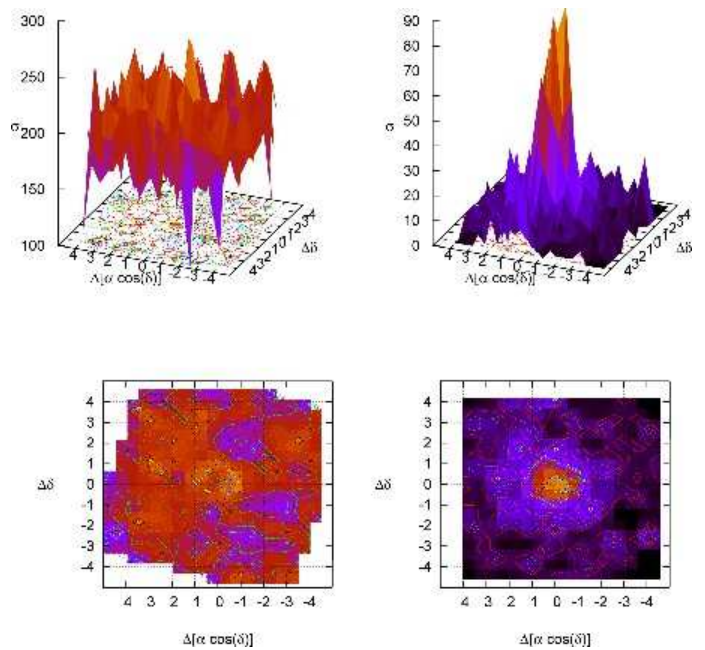


Fig. 2. Stellar surface-density σ (stars arcmin⁻²) of VVV CL036. The radial density profile produced with the raw photometry is shown to the left and the right images show the field after statistical decontamination.

total number of member stars N_{mem} and, repeating the above procedure for the 729 different setups, we obtained the average number of member stars $\langle N_{\text{mem}} \rangle$. Each star was ranked according to the number of times it survived after all runs (survival frequency) and only the $\langle N_{\text{mem}} \rangle$ highest ranked stars were taken as cluster members. For the present cases we obtained survival frequencies higher than 90%. Further details about the algorithm are described in Bonatto & Bica (2010). In Fig. 2 are shown the large-scale spatial distribution of the stellar surface-densities (σ , in units of stars arcmin⁻²) of VVV CL036, built with the raw (left panels), and field-star decontaminated (right) photometry. The decontaminated CMD of VVV CL036 is shown in Fig. 3.

5. Catalog of the Cluster Candidates

Preliminary analysis of the color-magnitude and color-color diagrams reveals 96 previously unknown star cluster candidates or young stellar groups. In Table 1 we list their basic properties. The first column of the table gives the identification followed by: the equatorial coordinates of the cluster candidate's center determined by eye, the number of most probable cluster members after statistical decontamination, eye-ball measured apparent cluster radius in arcsec, the VVV tile name, and comments about the nature of the object. The comments include details taken from the SIMBAD database such as: presence or absence of nebulousity (H II region) around the cluster; known nearby infrared, radio, and X-ray sources; young stellar objects (YSO); outflow candidates and masers. It should be noted that IRAS positions could have discrepancies of an arcminute or more (particularly if the sources are bright at 60–100 μm and not at 12–25 μm). Therefore we have listed IRAS sources within 100 arcsec of our detected clusters (and provided the separations of these with a proximity ≥ 10 arcsec).

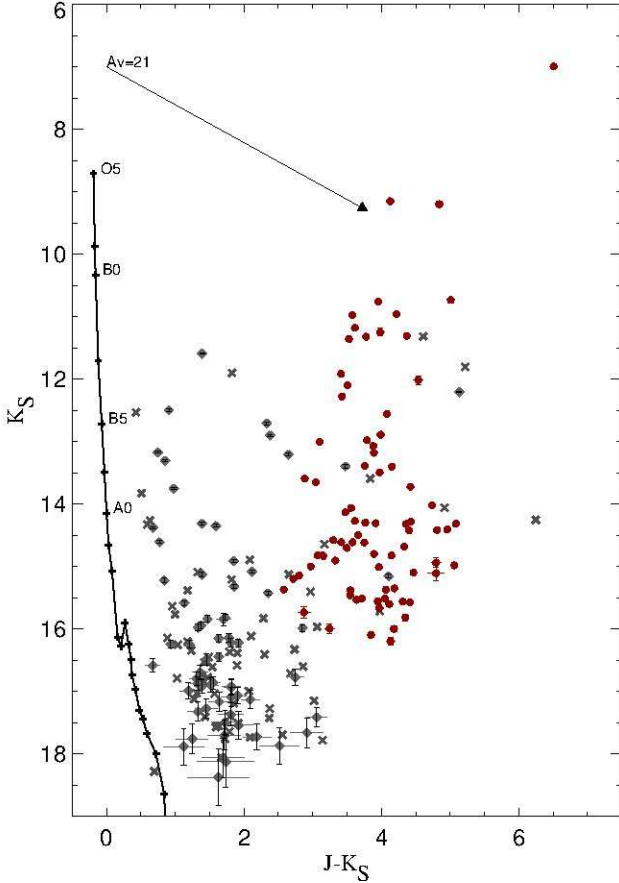


Fig. 3. VVV observed ($J - K_S$) vs. K_S CMD extracted from the $R = 0'.5$ region of VVV CL036. The most probable cluster members are plotted with filled circles and the filled rombs and crosses stand for the equal area two randomly selected comparison field stars. The continuous line represents the sequence of the zero-reddening stars of luminosity class V (Schmidt-Kaler 1982). Reddening vector for $A_V=21$ mag is also shown.

Fig. 4 shows JHK_S true color images of some of the newly discovered cluster candidates and stellar groups. The remainder are given in Appendix A.

The VVV survey area with the tile numbers is plotted in Fig. 5 with the new star cluster candidates from Table 1 overplotted. By the time of this work all disk tiles were available in the CASU database except those of d037 and d133, which represents 99% of the VVV disk area, or 248 deg^2 . The spatial distribution of the detected objects on the sky indicates that they are found mainly within Galactic longitude $l = \pm 1.5 \text{ deg}$ and shows two peaks in Galactic latitude at $l = 310$ and $330\text{--}340 \text{ deg}$.

During the visual inspection we rediscovered 50 of 96 star cluster candidates situated in the VVV disk area from the Dutra et al. (2003) catalog, 65 of 70 star cluster candidates from Mercer et al. (2005), as well as many clusters from WEBDA (Dias et al. 2002) database. The VVV true color images of three of them are given in Fig. 6. We did not identify any new cluster candidate similar to Westerlund 1 (right panel). However, it is hard to estimate the completeness of the catalog presented here with respect to the num-



Fig. 4. VVV JHK_S true color images of VVV open cluster candidates. The field of view is approx. 2.2×2.2 arcmin and North is to the left, East is up.



Fig. 6. The VVV JHK_S true color images of three known massive clusters. The field of view is 2.2×1.8 arcmin, 4.4×3.6 arcmin; 8.8×7.2 arcmin for DBSB 130, Mercer 77 and Westerlund 1, respectively.

ber of undiscovered clusters in the VVV disk area, as we focused our search towards known radio or mid-IR sources in order to identify young clusters with nebulosity and compact objects. These can be easily missed by automated search algorithms because the photometry in those regions is affected by abundant extended emission. Most probably the automated searches will discover many more less-concentrated cluster candidates, although they may still prove unreliable in providing a complete sample.

The cluster radii were measured by eye on the K_S 80 second VVV tile images. This method was preferred over automated algorithms, because the majority of our objects are embedded in dust and gas. The area around cluster candidates is smoothed and the density contours are overplotted with the lower limit of the contour equal to the density of comparison field. The mean radius of the sample is

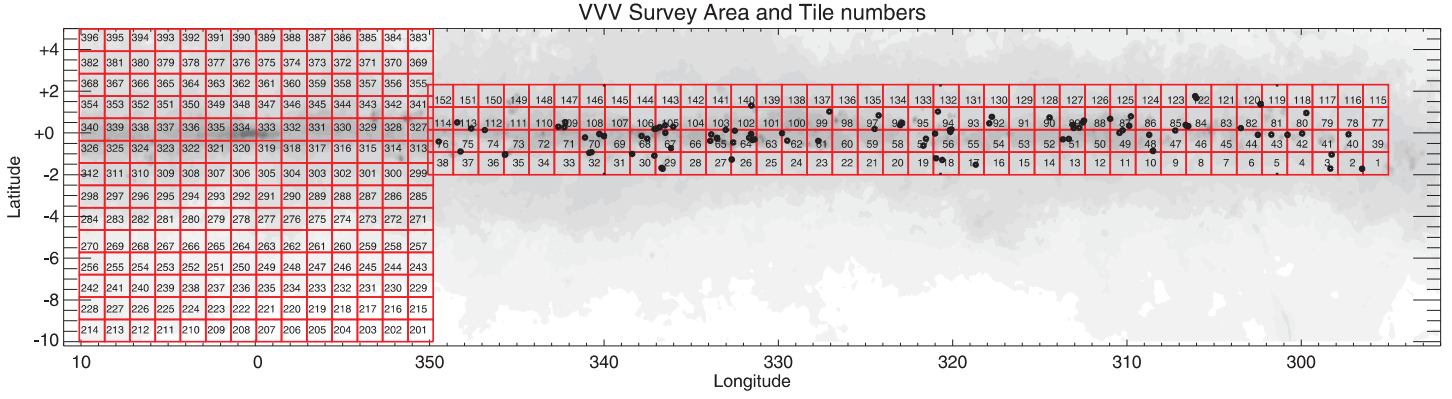


Fig. 5. The VVV Survey area, with individual tiles (see Minniti et al. 2010 for details) numbered. This is a plot of Galactic latitude b version Galactic longitude l , overplotted on a differential extinction contour map. The positions of the new star cluster candidates from Table 1 are marked.

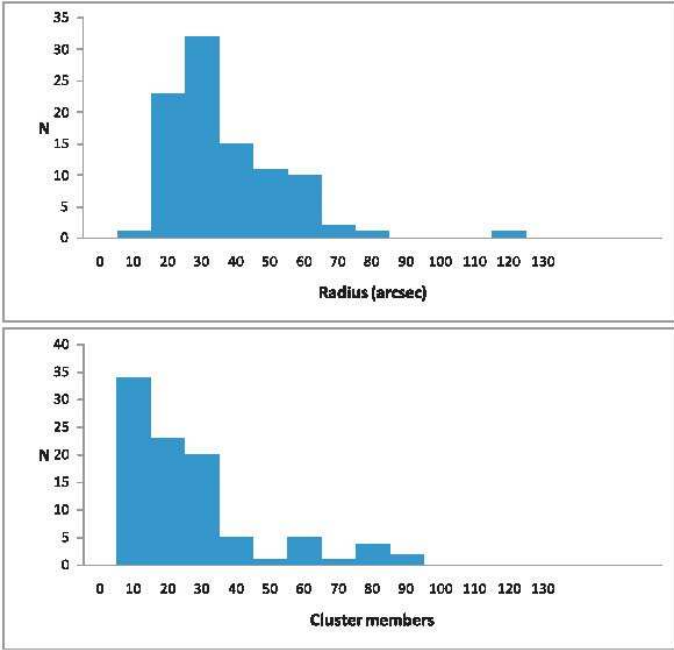


Fig. 7. Upper panel: Distribution of the detected objects with measured cluster radius (given in arcsec). Lower panel: Histogram of the cluster sample by number of most probable cluster members.

34 ± 18 arcsec. Here the uncertainty represents the standard deviation of the mean value. This calculated value is smaller than the mean values of 47 ± 17 arcsec, and 42 ± 22 arcsec, calculated for the Dutra et al. (2003) and Mercer et al. (2005) clusters respectively for the VVV disk area. The histogram of the number of star clusters vs. 10 arcsec binned radius is shown in Fig. 7. It can be seen that most of the clusters have a radius between 20 and 30 arcsec, clearly showing that deep infrared surveys such as VVV allow us to find new faint and compact (with small angular sizes) clusters.

Another possible indication of the richness of the clusters is the number of most probable cluster members, which are given in Column 4 of Table 1. We have to remind the reader however, that the cluster members are selected by statistical decontamination and the 90% completeness limit

of the decontaminated data is $K_S=15.5-16.5$ mag, dependant on crowding and differential reddening. The saturation of the brightest stars additionally complicates the situation, because in some cases it is not possible to replace them directly with 2MASS measurements. Often one 2MASS measurement represents 2 or 3 stars on the VVV images. All above comments have to be considered when determining the distribution of the cluster candidates by the number of most probable cluster members, shown in the lower panel of Fig. 7. This histogram presents a peak between 10–20 cluster members per cluster. Only 13 clusters have more than 50 members. The small number of cluster members, however, can be also due to the compact nature of the cluster, large distance and/or differential reddening.

The cluster nature of many of the objects listed in Table 1 needs to be confirmed with deeper high-resolution imaging and spectroscopy. Nevertheless we attempted to make some preliminary classification of the objects based on the morphology of decontaminated color-magnitude and color-color diagrams. Any additional information from the literature was also considered: a nebulosity associated with the object is interpreted as an indicator of youth if it is accompanied by a Main Sequence (MS) and/or Pre-Main Sequence (PMS) on the CMD. The presence of masers, radio, and IR sources within the bounds of the candidate, or of reddened fainter sources that might represent a PMS population, also indicate a young object. Fig. 8 shows a clear correlation between GLIMPSE dust structures and projected position of our star cluster candidates.

According to Plante & Sauvage (2002) the typical age of embedded clusters is between 1 and 4 Myr, while the classical open clusters have ages from 10^6 to $\sim 10^9$ years. Thus, the candidates with a MS, but lacking any signatures of youth, are considered as classical open clusters with their ages needing to be determined by isochrone fitting. According to the last column of Table 1, 80 of 96 of our clusters are embedded or very close to nebulosity, while in most of the cases IR, radio, maser, and/or YSO sources are located nearby according to the SIMBAD database. Thus, we infer from the proximity to these sources that $\sim 85\%$ of cluster candidates and stellar groups are younger than 5 Myr. This is in agreement with a Galactic disk active in star formation model.

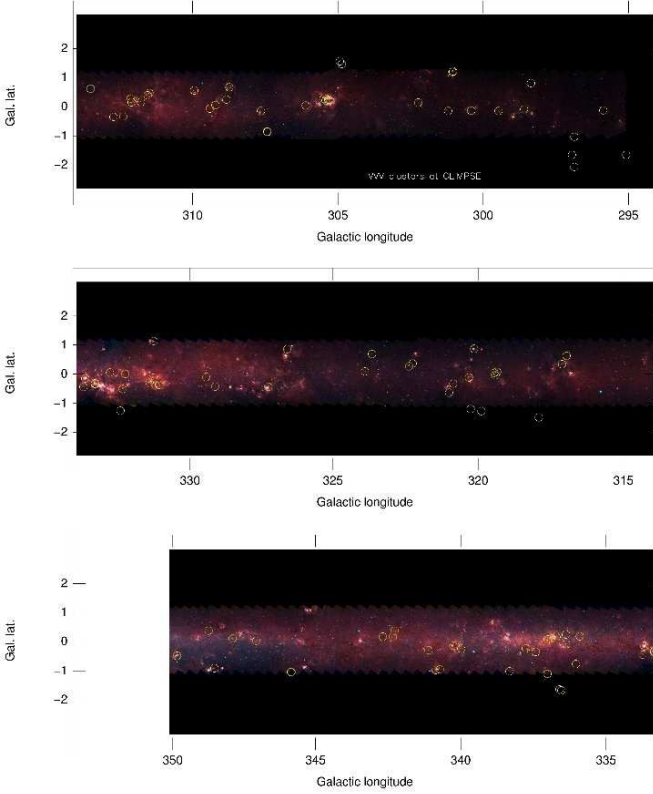


Fig. 8. The VVV disk survey area, overplotted on the GLIMPSE 3.6, 4.5 and 8.0 μm true color image, with the new star cluster candidates positions.

6. Parameters of some VVV cluster candidates

Visible and near-IR data, both imaging and spectroscopy, are normally needed to characterize the main physical parameters of the cluster population (Hillenbrand 1997). Unfortunately, our cluster candidates are practically invisible in the optical. However, follow-up spectroscopy is in progress in the near-IR. As we have at our disposal the near-infrared color-magnitude and color-color diagrams, we can obtain some initial estimates of basic cluster parameters such as reddening, distance, and age. But we note that this is only particularly effective for the relatively well populated cluster candidates.

The mean reddening (interstellar absorption) is well determined from the $J-H$ vs. $H-K_S$ color-color diagram. To illustrate the process we show in Fig. 9 the decontaminated $J-H$ vs. $H-K_S$ color-color diagram of VVV CL062. The intrinsic colors of the MS stars (Schmidt-Kaler 1982) and giant branch (Koornneef 1983) are overplotted. The reddening vectors (Bessell et al. 1998) which encompass the MS stars correspond to a visual extinction of 15 magnitudes. Clearly, Fig. 9 indicates that most of the stars are reddened main-sequence stars. The color spread of cluster members, however, is much larger than the typical photometric errors of 0.05 mag, suggesting large differential extinction. The locus lies between the two parallel dotted lines and the calculated mean value and the standard deviation of the fit for this cluster are $A_V=14.7\pm 0.9$ mag. Sources located to the right and below the reddening line

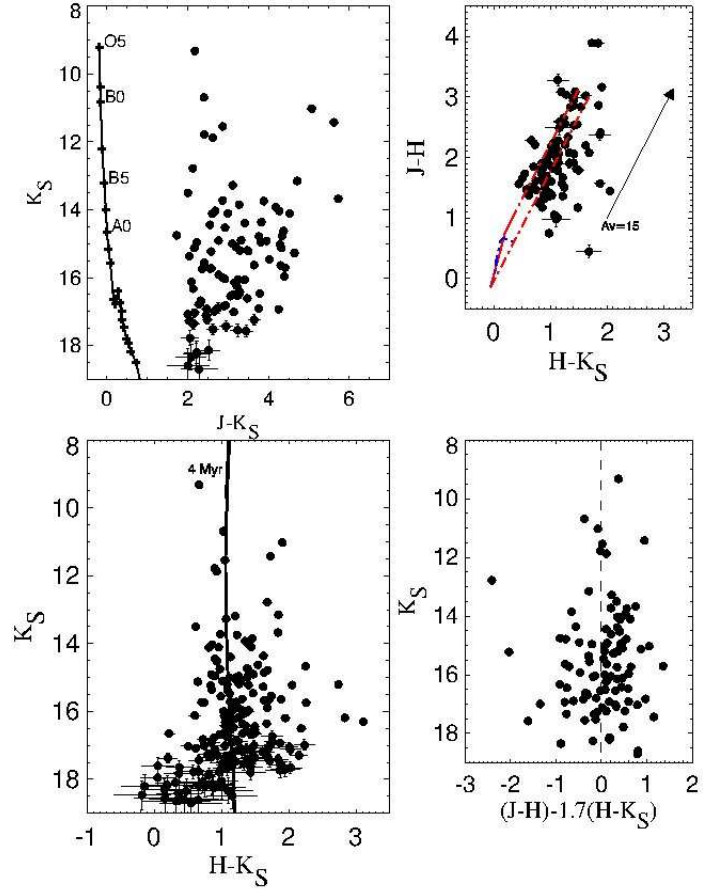


Fig. 9. VVV observed CMDs extracted from the $R \leq 0.8$ region of VVV CL062. The top-left panel shows statistically decontaminated most probable cluster members with the Schmidt-Kaler (1982) sequence in the $(J-K_S)$ vs. K_S diagram. The top-right panel gives $(J-H)$ vs. $(H-K_S)$ color-color diagram. The continuous lines represent the sequence of the zero-reddening stars of luminosity class I (Koornneef 1983) and class V (Schmidt-Kaler 1982). The reddening vector for $A_V = 15$ mag is overplotted and the dotted lines are parallel to the standard reddening vector. The bottom-left panel shows the $(H-K_S)$ vs. K_S color-magnitude diagram with a 4 Myr isochrone from Girardi et al. (2010). In the bottom-right panel the reddening free color of $(J-H) - 1.70(H-K_S)$ is plotted vs. K_S magnitude.

may have excess emission in the near infrared (IR-excess sources) and/or may be pre-main sequence stars.

Most of the objects in our catalog are young and highly obscured/extinguished clusters (see Table 1). The clusters younger than ~ 30 Myr are expected to be affected by differential internal reddening. Indeed, Yadav & Sagar (2001) show that differential reddening tends to increase towards younger ages, in some cases reaching ΔA_V up to 3 mag. Unfortunately, we do not yet have enough information to be able to simply estimate the level of differential reddening, as the characteristics of the ISM near the clusters, as well as the profile of extinction between us and the clusters are

unknown. If all the extinction is due to a non-uniform thin screen immediately in front of a cluster, then the standard deviation of the extinction to each star (i.e. the measurement of differential reddening) could be as much as twice the mean extinction of stars within the cluster (Fischera & Dopita 2004). If a cluster is embedded in a cloud which produces much of the extinction along the line of sight to the cluster, we would not only get a contribution to differential extinction from the angular position of each star, but also from its distance, as more distant stars would be, on average, more heavily extinguished.

We attempt to negate the effect of differential reddening by employing the reddening free parameter $Q = (J - H) - 1.70(H - K_S)$, as defined by Negueruela et al. (2007) for OB stars (see also Catelan et al. 2011, for a list of several other reddening-free indices, in the ZYJHK system). We chose this parameter in order to avoid the intrinsic degeneracy between reddening and spectral type (and since we expect to find early OB stars in the majority of the clusters in our sample). The bottom-right panel of Fig. 9 shows this reddening free parameter vs. K_S magnitude. According to Negueruela et al. (2007) the OB stars will have $Q \simeq 0.0$ in the diagram, whilst stars with $Q < -0.05$ and large values of $(J - K_S)$ can be classified as infrared excess objects and therefore PMS candidates. The preliminary separation between reddened OB stars and PMS stars can be very useful for analysis of the color-magnitude diagrams and especially for isochrone fitting.

In general, without the distance of at least 2-3 cluster members having been estimated by spectroscopic parallax and/or knowledge of differential reddening, measurement of the distance and age using only IR photometry is uncertain. Therefore we give only initial estimates for these parameters that can be used for some studies, but that must be confirmed with follow up observations.

The photometric distance and age can be estimated simultaneously by fitting the observed color-magnitude diagram with solar-metallicity Padova isochrones (Girardi et al. 2010) computed with the 2MASS J , H , and K_s filters. Starting with the isochrones set to zero distance modulus and reddening, we apply shifts in magnitude and color until the fitting statistics reach a minimum value (i.e. difference in magnitude and color of the stars from the isochrone should be minimal). The closest, younger and older fitting solutions were used to provide the age uncertainties. To avoid the dependence of such calculated uncertainties on the resolution of the model grid used, we adopted the largest, most conservative value as the error of age determination. Fig. 10 shows the adopted fits superimposed on the decontaminated CMDs for some of the clusters. Parameters derived from the isochrone fit are the true distance modulus $(m - M)_0$, age, and reddening $E(J - K_S)$. Reddening estimates can be converted to $E(B - V)$ and A_V using the equations $E(J - K_S) = 0.56 \times E(B - V)$ and $A_{K_S} / A_V = 0.118$, which assume $A_V = 3.1 \times E(B - V)$ (Dutra et al. 2002). These estimates are presented in Table 2.

7. Summary

In this paper we report the discovery of 96 near-infrared open clusters and stellar groups, found in the Galactic disk area using the ‘‘VVV – Vista Variables in the Vía Láctea’’ ESO Large Survey. Our search concentrated in the direc-

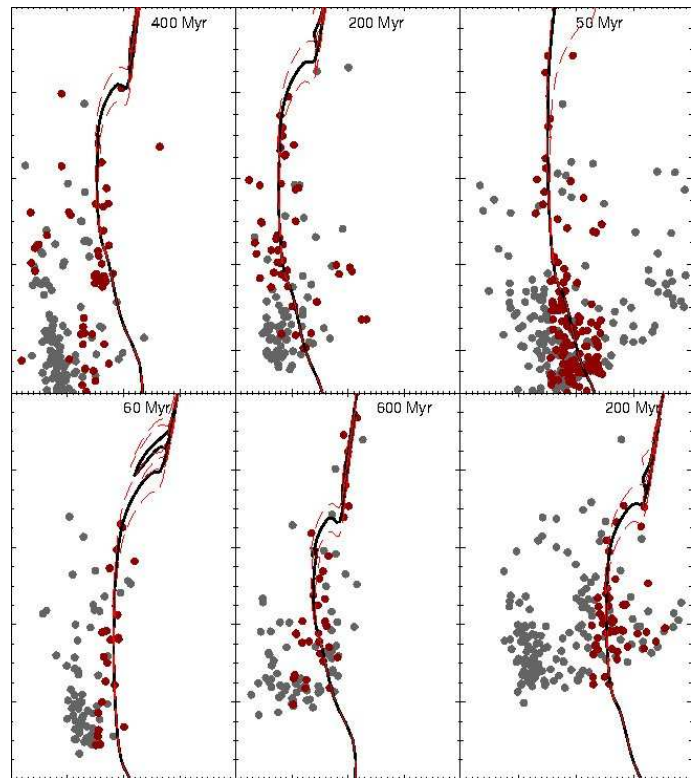


Fig. 10. VVV CMDs of (from upper left to bottom right) VVV CL008, VVV CL009, VVV CL039, VVV CL047, VVV CL070, VVV CL095. The statistically decontaminated CMDs are shown as red filled circles, the comparison field as gray filled circles. The best isochrone fit (Girardi et al. 2010) is plotted as a solid line, while the dotted lines represent the closest younger and older solutions.

tions of known star formation regions, masers, radio, and infrared sources.

The statistics of the foreground reddening of the known Galactic open clusters (e.g. WEBDA, and Fig. 4 of Bonatto et al. 2006) shows that by far the majority of them have $A_V \leq 3$ mag, with very few having $A_V = 5-6$ mag. Table 2 shows that VVV is really digging deep in the dust, with a mean $A_V = 11$ mag and reaching values of $A_V = 20$ mag. This highlights the potential of the VVV survey for finding new open clusters, especially those hiding in dusty regions. Most of the new cluster candidates are faint and compact (with small angular sizes) having radii between 20 and 30 arcsec. An automated search for less-concentrated candidates over the whole VVV area (bulge and disk) based on the color cuts algorithm (Ivanov et al. 2010) is in progress.

Due to our search being directed towards star formation regions along the Southern Galactic plane we found (based on the preliminary photometric analysis) that approximately 85% of the star cluster candidates are younger than 5 Myr. It is hard to estimate the masses of the clusters without accurate distance and age determinations. Taking into account the number of most probable cluster members however, it seems that most of them are intermediate or low mass clusters ($< 10^3 M_\odot$). Spectroscopic follow-up is in progress to verify this, and to derive the spectral types and distances of brighter cluster members. Once completed, our

Table 2. Parameters of relatively well populated VVV cluster candidates.

Name	A_V mag	$(m - M)_0$ mag	Dist. kpc	Age Myr
VVV CL008	8.3 ± 0.5	10.7 ± 0.7	1.4 ± 0.5	400 ± 50
VVV CL009	4.5 ± 0.3	11.9 ± 0.6	2.4 ± 0.5	200 ± 40
VVV CL039	8.8 ± 0.5	11.5 ± 0.9	2.0 ± 0.7	75 ± 40
VVV CL041	8.8 ± 0.6	9.8 ± 0.7	0.9 ± 0.5	$25 - 30$
VVV CL047	10.5 ± 0.9	14.5 ± 1.3	7.9 ± 1.3	60 ± 30
VVV CL059	20.0 ± 1.4	10.5 ± 0.8	1.3 ± 0.5	$20 - 30$
VVV CL070	7.2 ± 0.3	11.5 ± 1.4	2.0 ± 0.9	600 ± 40
VVV CL095	13.9 ± 1.9	12.4 ± 0.8	3.0 ± 1.4	200 ± 40
VVV CL099	13.4 ± 1.6	9.2 ± 0.7	0.7 ± 0.6	$20 - 50$
VVV CL100	14.6 ± 1.2	13.2 ± 1.4	4.3 ± 1.1	$5 - 10$

subsequently constructed homogeneous sample will allow us to better trace the star formation process in the inner Galactic disk.

Acknowledgements. JB is supported by FONDECYT No.1080086 and by the Ministry for the Economy, Development, and Tourism's Programa Inicativa Científica Milenio through grant P07-021-F, awarded to The Milky Way Millennium Nucleus. The data used in this paper have been obtained with VIRCAM/VISTA at the ESO Paranal Observatory. The VVV Survey is supported by the European Southern Observatory, by BASAL Center for Astrophysics and Associated Technologies PFB-06, by FONDAP Center for Astrophysics 15010003, by the Ministry for the Economy, Development, and Tourism's Programa Inicativa Científica Milenio through grant P07-021-F, awarded to The Milky Way Millennium Nucleus. This publication makes use of data products from the Two Micron All Sky Survey, which is a joint project of the University of Massachusetts and the Infrared Processing and Analysis Center/California Institute of Technology, funded by the National Aeronautics and Space Administration and the National Science Foundation. This research has made use of the Aladin and SIMBAD database, operated at CDS, Strasbourg, France. RK acknowledges support from Cento de Astrofísica de Valparaíso and DIPUV 23/2009. We express our thanks to the anonymous referee for very helpful comments. SLF acknowledges funding support from the ESO-Government of Chile Mixed Committee 2009, and from GEMINI Conicyt grant No. 32090014/2009. DM and DG acknowledge support from FONDAP Center for Astrophysics No. 15010003. DM is supported by FONDECYT No. 1090213. CB and EB acknowledge support from Brazil's CNPq. JRAC is supported by GEMINI-CONICYT FUND No.32090002. RdG acknowledges partial research support through grant 11073001 from the National Natural Science Foundation of China. D.G. gratefully acknowledges support from the Chilean Centro de Excelencia en Astrofísica y Tecnologías Afines (CATA). MSNK is supported by a Ciência 2007 contract, funded by FCT/MCTES (Portugal) and POPH/FSE (EC). JRAC, SES, JAG, FP are supported by the Ministry for the Economy, Development, and Tourism's Programa Inicativa Científica Milenio through grant P07-021-F, awarded to The Milky Way Millennium Nucleus. ANC received support from Comitee Mixto ESO-GOBIERNO DE CHILE 2009. ANC and RB are supported by BASAL Center for Astrophysics and Associated Technologies PFB-06. R.S. acknowledges financial support from CONICYT through GEMINI Project No. 32080016. RB acknowledges support from Gemini-CONICYT project 32080001, and DIULS PR09101.

References

- Arnaboldi, M., Neeser, M. J., Parker, L. C., et al. 2007, *Messenger*, 127, 28
- Artigau, É., Radigan, J., Folkes, S., et al. 2010, *ApJ*, 718, L38 *A&A*, 333, 231
- Benjamin, R., Churchwell, E., Babler, B., et al. 2003, *PASP*, 115, 953
- Bessell, M.S., Castelli, F., & Plez, B. 1998,
- Bica, E., Dutra, C.M., Soares, J., Barbuy, B. 2003, *A&A*, 404, 223
- Bonatto C. & Bica E. 2010, *A&A*, 516, 81
- Bonatto C., Kerber L.O., Bica E. & Santiago B.X. 2006, *A&A*, 44, 121
- Borissova, J., Pessev, P., Ivanov, V.D. et al. 2003, *A&A*, 411, 83
- Borissova, J., Ivanov, V.D., Minniti, D. et al. 2005, *A&A*, 435, 95
- Borissova, J., Ivanov, V.D., Minniti, D., & Geisler, D. 2006, *A&A*, 455, 923
- Borissova, J., Ivanov, V.D., Hanson, M.M., et al. 2008, *A&A*, 488, 151
- Borissova, J., Kurtev, R., & Ivanov, V. D. 2009, *RMxAC*, 35, 54
- Borissova, J., Kurtev, R., Hanson, M. M., et al. 2010, *IAU Symposium*, 266, 366
- Catelan, M., et al. 2011, in *Carnegie Observatories Astrophysics Series*, Vol. 5, RR Lyrae Stars, Metal-Poor Stars, and the Galaxy, ed. A. McWilliam (arXiv:1105.1119)
- Churchwell, E., Povich, M., Allen, D., et al. 2006, *ApJ*, 649, 759
- Churchwell, E., Watson, D., Povich, M., et al. 2007, *ApJ*, 670, 428
- Dalton, G. B., Caldwell, M., Ward, A. K., et al. 2006, *Ground-based and Airborne Instrumentation for Astronomy*. Edited by McLean, Ian S. & Iye, Masanori., *Proceedings of the SPIE*, 6269, 30
- Depoy, D., Atwood, B., Byard, P., Frogel, J., & O'Brien, Th. 1993, *Infrared Detectors and Instrumentation*, Albert M. Fowler ed, *Proceedings of the SPIE*, 1946, 667,
- de Wit, W., Testi, L., Palla, F., & Zinnecker, H. 2005, *A&A*, 437, 247
- Dias W. S., Alessi B. S., Moitinho A. & Lepine J. R. D., 2002, *A&A*, 389, 871
- Dutra C.M., Santiago B.X. & Bica E. 2002, *A&A*, 383, 219
- Dutra, C.M., Bica, E., Soares, J., & Barbuy, B., 2003, *A&A*, 400, 533
- Fischera, J., & Dopita, M. A. 2004, *ApJ*, 611, 919
- Froebich, D., Scholz, A., Raftery, C.L., 2007, *MNRAS*, 374, 399
- Froebich, D., Meusinger, H., & Scholz, A. 2007, *MNRAS*, 377, L54
- Girardi, L., Williams, B., Gilbert, K., Rosenfield, P., & Dalcanton, J. 2010, *ApJ*, 724, 1030
- Glushkova, E., Kopusov, S., Zolotukhin, I., Beletsky, Yu., Vlasov, A., Leonova, S. 2010, *Astronomy Letters*, 36, 75
- Hanson, M. M., & Bubnick, B. F, 2008, *PASP*, 120, 150
- Hanson, M. M., Kurtev, R., Borissova, J., et al. 2010, *A&A*, 516, 35
- Hanson, M. M. 2003, *ApJ*, 597, 957
- Hillenbrand, L. A. 1997, *AJ*, 113, 1733
- Irwin, M. Lewis, J., Hodgkin, S., et al. 2004, *Optimizing Scientific Return for Astronomy through Information Technologies*. Edited by Quinn, Peter J. & Bridger, Alan, *Proceedings of the SPIE*, 5493, 411
- Ivanov, V.D., Borissova, J., Pessev, P., et al. 2002, *A&A*, 349, 1
- Ivanov, V.D., Kurtev, R., & Borissova, J. 2005, *A&A*, 442, 195
- Ivanov, V. D., Messineo, M., Zhu, Q., et al. 2010, *IAU Symposium*, 266, 203
- Ivanov, V.D., Messineo, M., Zhu, Q., et al. 2011, *A&A*, submitted
- Koornneef, J. 1983, *A&A*, 128, 84
- Kurtev, R., Borissova, J., Georgiev, L., Ortolani, S., & Ivanov, V.D., 2007, *A&A*, 475, 209
- Kurtev, R., Ivanov, V.D., Borissova, J., & Ortolani, S., 2008, *A&A*, 2008, 489, 586
- Kurtev, R., Borissova, J., Ivanov, V. D., & Georgiev, L. 2009, *RMxAC*, 35, 160
- Lada, C.J., & Lada, E.A., 2003, *ARA&A*, 41, 57 of *London Philosophical Transactions Series A*, 368, 713

- Lamers, H.J.G.L.M., Gieles, M., Bastian, N., et al. 2005, *A&A*, 117, 129
- Longmore, S. N., & Burton, M. G 2009, *PASA*, 26, 439
- Longmore, A., Kurtev, R., Lucas, P., Froebrich, D., R. de Grijs et al. 2011, *MNRAS*, in press
- Mercer, E., Clemens, D., Meade, M., et al. 2005, *ApJ*, 635, 560
- Minniti, D., Lucas, P., Emerson, J., et al. 2010, *New A*, 15, 433;
- Minniti, D., Hempel, M., Toledo, I., et al. 2011, *A&A*, 527, 81
- Mottram, J. C., Hoare, M. G., Lumsden, S. L., et al. 2007, *A&A*, 476, 1019
- Negueruela, I., Marco, A., Israel, G. L., & Bernabeu, G. 2007, *A&A*, 471, 485
- Piskunov, A., Schilbach, E., Kharchenko, N. V., Roser, S., & Scholz, R. 2008, *A&A*, 477, 165
- Plante, S. & Sauvage, M., 2002, *AJ*, 124, 1995
- Portegies Zwart, S., McMillan, S., & Gieles, M. 2010, *ARA&A*, 48, 431
- Robberto, M., Soderblom, D. R., Scandariato, G., Smith, K., Da Rio, N., Pagano, I., & Spezzi, L. 2010, *AJ*, 139, 950
- Saito, R., Hempel, M., Alonso-Garcia, J., et al. 2010, *The Messenger*, vol. 141, 24
- Schmidt-Kaler, T., 1982, in *Landolt-Borstein, New Series, Group VI*, vol. 2, ed. K. Schaifers & H.H. Voigt (Berlin: Springer-Verlag),1
- Siess, L., Dufour, E., & Forestini, M. 2000, *A&A*, 358, 593
- Skrutskie, M., Cutri, R.M., Stiening, R., et al. 2006, *AJ*, 131, 1163
- Stetson, P. 1987, *PASP*, 99, 191
- Yadav R.K.S. & Sagar R. 2001, *MNRAS*, 328, 370

Table 1. VVV Cluster Candidates

Name	RA(J2000) hh:mm:ss	DEC(J2000) deg:mm:ss	Numb.	Radius arcsec	Tile	Comments
VVV CL005	11:38:59	-63:28:44	25	24	d001	nebulousity, embedded; partofcloud:[SMN83] Lam Cen I; Be star
VVV CL006	11:49:12	-62:12:27	12	30	d039	weak nebulousity, embedded; faint; MSX6C G295.7483-00.2076
VVV CL007	11:53:51	-64:20:30	15	20	d002	weak nebulousity, embedded; IR:IRAS 11513-6403
VVV CL008	11:55:29	-63:56:24	25	37	d002	no nebulousity; overdensity
VVV CL009	11:56:03	-63:18:57	30	35	d002	no nebulousity; overdensity
VVV CL010	12:11:47	-61:46:23	10	28	d079	strong nebulousity, embedded:GAL 298.26+00.74;IR-[HSL2000] IRS 1; Mas:Caswell CH3OH 298.26+00.74; stellar group; outflow; very red
VVV CL011	12:12:41	-62:42:31	16	6	d041	no nebulousity; very concentrated
VVV CL012	12:20:14	-62:53:04	15	37	d042	nebulousity, embedded; small; IR:IRAS 12175-6236
VVV CL013	12:28:37	-62:58:25	15	27	d042	nebulousity, embedded; YSO:G300.3412-00.2190
VVV CL014	14:19:09	-60:30:46	60	30	d089	no nebulousity; overdensity; IR:IRAS14153-6018 (83" away)
VVV CL015	12:34:52	-61:40:16	10	20	d119	nebulousity, embedded; very close to DBSB 77 - part of DBSB 77 or triggered?; IR:Caswell H2O 300.97+01.14
VVV CL016	12:35:00	-61:41:40	10	40	d119	nebulousity, embedded; close to DBSB 77; young cluster+ SF on the border
VVV CL017	12:35:35	-63:02:39	10	30	d043	nebulousity, embedded:GAL 301.12-00.20;IR; Mas:Caswell H2O 301.14-00.23
VVV CL018	12:44:40	-62:47:46	25	30	d082	nebulousity, embedded; IR:IRAS 12417-6231
VVV CL019	13:07:06	-61:25:03	10	50	d121	nebulousity; YSOs; stellar group
VVV CL020	13:07:36	-61:19:28	13	24	d121	no nebulousity; several stars
VVV CL021	13:11:51	-62:36:52	8	29	d084	weak nebulousity; stellar group; Rad:DWS84 G305.27+0.17
VVV CL022	13:12:36	-62:37:16	8	53	d084	nebulousity, embedded; red; Mas:Caswell OH 305.362+00.150
VVV CL023	13:13:13	-62:33:26	15	27	d084	nebulousity, embedded; IR:IRAS 13100-6217
VVV CL024	13:18:45	-62:44:39	8	27	d084	nebulousity, embedded; close to DBSB 85; IR:IRAS 13154-6228A
VVV CL025	13:31:22	-63:28:27	5	17	d047	weak nebulousity, embedded; faint; IR:IRAS 13280-6312 (35" away)
VVV CL026	13:31:26	-63:27:52	7	18	d047	weak nebulousity, embedded; faint; IR:IRAS 13280-6312
VVV CL027	13:32:24	-62:43:39	40	13	d047	close to nebulousity; overdensity
VVV CL028	13:40:23	-61:44:00	10	12	d086	stellar group; very close to C 1336-614(BH 151); concentrated
VVV CL029	13:41:54	-62:07:38	20	27	d086	nebulousity, embedded; IR:IRAS 13384-6152
VVV CL030	13:45:28	-62:14:33	5	20	d086	nebulousity, embedded; faint group; IR:IRAS 13419-6159
VVV CL031	13:47:20	-62:18:44	15	45	d049	weak nebulousity; overdensity; masers; IR:IRAS 13438-6203
VVV CL032	13:50:41	-61:35:13	15	54	d087	nebulousity:GAL 309.92+00.48, embedded, very red stars; YSO:DZOA 4655-11; DkNeb; 6 Mas
VVV CL033	14:03:27	-61:16:13	7	27	d088	nebulousity, embedded; stellar group
VVV CL034	14:04:08	-61:19:55	5	34	d088	nebulousity, embedded; stellar group
VVV CL035	14:06:27	-61:29:35	8	28	d088	nebulousity, embedded; stellar group
VVV CL036	14:09:03	-61:16:02	52	50	d088	no nebulousity; overdensity; IR:IRAS 14054-6102
VVV CL037	14:09:07	-61:24:43	15	43	d088	nebulousity, embedded; IR:IRAS 14054-6110
VVV CL038	14:12:44	-61:47:06	10	20	d051	nebulousity, embedded; faint; IR:IRAS 14090-6132
VVV CL039	14:15:32	-61:41:47	72	60	d051	no nebulousity; 2E 1412.0-6127 (X-ray source at 91")
VVV CL040	14:44:22	-59:11:47	20	32	d092	faint; no nebulousity
VVV CL041	14:46:26	-59:23:17	51	54	d092	no nebulousity; overdensity; IR:IRAS 14428-5911 (92" away)
VVV CL042	14:58:48	-60:40:07	25	74	d016	no nebulousity; several bright stars
VVV CL043	15:02:56	-58:35:55	25	54	d055	weak nebulousity; overdensity; close to Mercer 58
VVV CL044	15:03:40	-58:35:07	10	40	d093	no nebulousity; several bright stars
VVV CL045	15:03:47	-58:40:11	10	54	d093	no nebulousity; several bright stars; IR:IRAS 14598-5823 (12" away)
VVV CL046	15:10:08	-58:17:06	15	20	d056	nebulousity, embedded; close DBSB 139, triggered?
VVV CL047	15:11:52	-59:30:30	22	21	d018	no nebulousity; faint stars
VVV CL048	15:14:01	-59:15:13	10	27	d018	weak nebulousity, embedded; IR:IRAS 15100-5903
VVV CL049	15:14:30	-58:11:49	68	30	d056	no nebulousity; IR:IRAS 15107-5800 (86" away)
VVV CL050	15:21:06	-57:57:32	12	15	d057	weak nebulousity, embedded; faint stars

Table 1. continued.

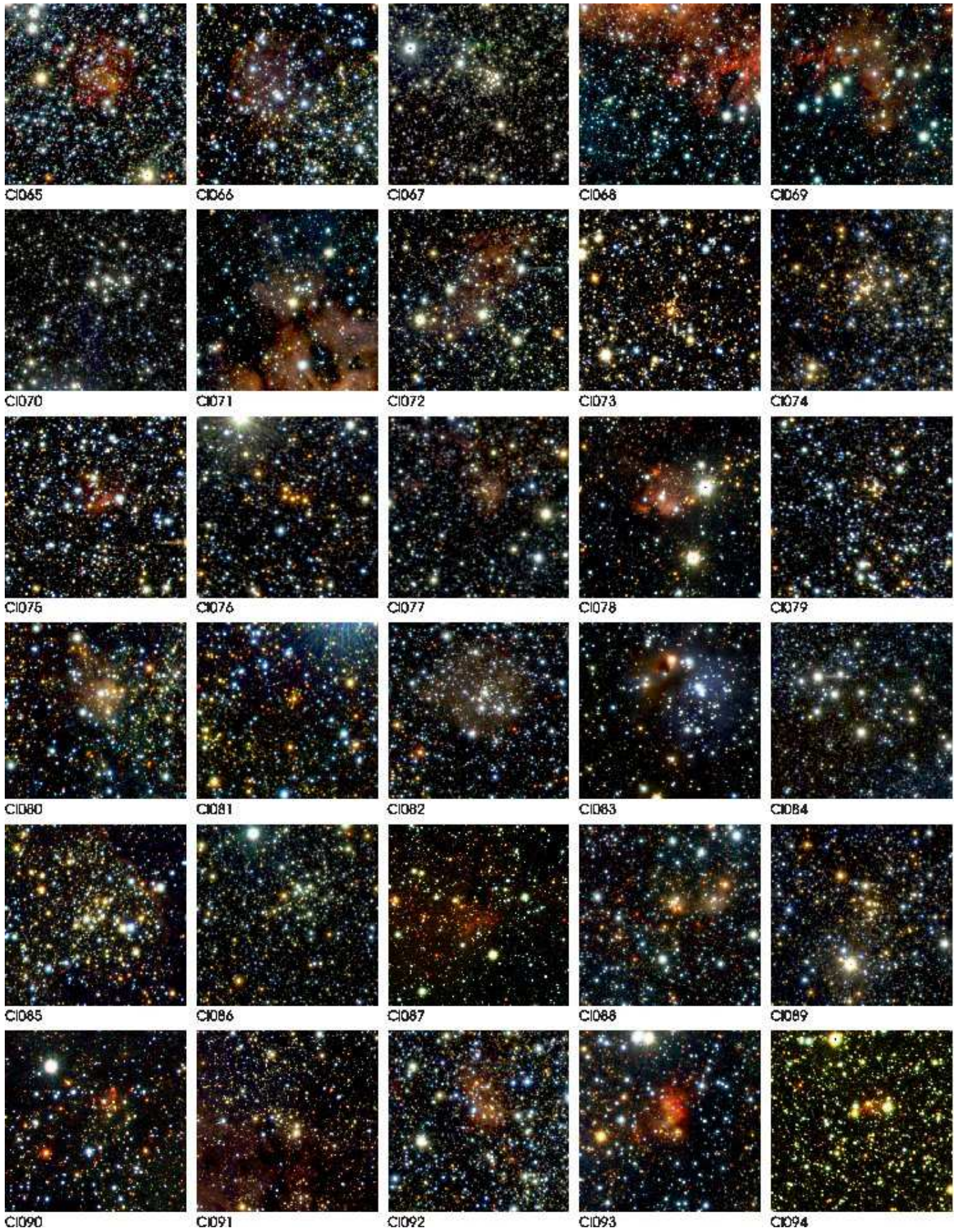
Name	RA(J2000) hh:mm:ss	DEC(J2000) deg:mm:ss	Numb.	Radius arcsec	Tile	Comments
VVV CL051	15:20:39	-56:51:37	45	50	d095	no nebulosity; overdensity
VVV CL052	15:21:44	-56:52:40	21	36	d095	weak nebulosity, embedded; IR:IRAS 15178-5641
VVV CL053	15:27:45	-55:48:38	38	78	d096	weak nebulosity; several bright stars
VVV CL054	15:31:36	-56:10:20	29	54	d097	weak nebulosity; IR:IRAS 15277-5600
VVV CL055	15:43:36	-53:57:52	10	15	d098	weak nebulosity; of?:EGO G326.61+0.80, stellar group
VVV CL056	15:52:38	-54:34:38	10	27	d061	nebulosity; small; very close to DBSB 146, triggered?
VVV CL057	16:02:11	-53:22:37	10	14	d062	nebulosity; small; IR:IRAS 15583-5314, stellar group
VVV CL058	16:02:19	-52:55:28	20	28	d062	nebulosity, IR:IRAS 15584-5247; Mas; YSOcand
VVV CL059	16:05:52	-50:47:49	35	45	d102	nebulosity; IR:IRAS 16021-5039
VVV CL060	16:11:23	-51:42:49	10	48	d064	nebulosity:[KC97c]; Rad:G331.3-00.2, GAL 331.26-00.19; stellar group
VVV CL061	16:11:28	-52:01:33	8	22	d063	nebulosity; stellar group; IR:IRAS 16076-5154
VVV CL062	16:12:08	-51:58:08	74	39	d063	nebulosity; IR:IRAS 16082-5150
VVV CL063	16:12:42	-51:45:03	10	21	d064	nebulosity; IR:IRAS 16089-5137
VVV CL064	16:15:18	-50:56:48	30	28	d102	weak nebulosity; faint
VVV CL065	16:17:31	-50:32:30	25	32	d103	nebulosity:IR:IRAS 16137-5025; YSO:[MHL2007] G332.7673-00.0069 1; very close to Mercer 77
VVV CL066	16:17:59	-51:15:10	7	49	d064	nebulosity; small; overdensity; IR:IRAS 16141-5107
VVV CL067	15:10:36	-57:54:41.77	30	30	d094	no nebulosity; concentrated
VVV CL068	16:21:28	-50:26:24	8	10	d065	nebulosity:GAL 333.29-00.37; stellar group, at the border of DBSB 165 triggered?
VVV CL069	16:21:34	-50:27:29	13	60	d065	nebulosity; SFR?
VVV CL070	16:21:48	-51:44:11	30	26	d026	no nebulosity; overdensity
VVV CL071	16:22:16	-50:04:30	14	25	d065	at the border of strong nebulosity, very close to [BDB2003] G333.60-00.21
VVV CL072	16:23:49	-50:14:20	19	58	d065	nebulosity; IR:IRAS 16200-5007
VVV CL073	16:30:24	-48:13:06	38	20	d105	no nebulosity
VVV CL074	16:32:06	-47:49:32	87	33	d105	no nebulosity; overdensity; Dark Cloud SDC G336.381+0.190
VVV CL075	16:33:30	-48:03:35	12	27	d067	weak nebulosity:GRS 336.37 -00.13; IR:MSX5C G336.3618-00.1373; Mas:[HLB98] SEST 107
VVV CL076	16:33:48	-47:38:49	10	20	d105	5-6 bright stars with the same color
VVV CL077	16:34:48	-47:32:49	21	15	d105	nebulosity; IR:IRAS 16311-4726
VVV CL078	16:35:09	-48:46:24	22	41	d067	nebulosity; IR:IRAS 16313-4840 -nebulosity
VVV CL079	16:35:22	-47:28:33	18	15	d105	no nebulosity, stellar group, X:SSTGLMC G337.0012+00.0305
VVV CL080	16:38:56	-47:27:01	22	25	d068	weak nebulosity; IR:IRAS 16352-4721
VVV CL081	16:39:43	-47:06:57	29	10	d068	no nebulosity; very red stars, or dust window?
VVV CL082	16:40:39	-48:16:07	30	34	d030	weak nebulosity, embedded; IR:2MASS J16412047-4900172
VVV CL083	16:41:19	-49:00:42	30	46	d029	nebulosity, embedded; YSO:[MHL2007] G336.5299-01.7344 2, [MHL2007] G336.5299-01.7344 3, 2MASS J16412047-4900172
VVV CL084	16:41:24	-48:56:33	15	50	d029	no nebulosity, but close; several bright stars
VVV CL085	16:45:26	-47:13:02	37	40	d068	no nebulosity
VVV CL086	16:48:15	-45:26:06	72	35	d070	no nebulosity; overdensity; MX5C G340.0160-00.3041
VVV CL087	16:48:50	-45:09:32	10	60	d070	nebulosity; small overdensity
VVV CL088	16:52:34	-44:36:07	17	12	d070	close to nebulosity; very concentrated; 5 YSO
VVV CL089	16:53:47	-43:16:03	83	34	d109	close to nebulosity; overdensity
VVV CL090	16:54:03	-45:18:53	8	14	d070	nebulosity; stellar group; YSO:[MHL2007] G340.7455-01.0021; close to DBSB 106
VVV CL091	16:54:39	-45:14:09	10	80	d070	weak nebulosity; overdensity
VVV CL092	16:54:56	-43:21:46	10	27	d109	nebulosity:[WHR97] 16513-4316A ; stellar group
VVV CL093	16:56:03	-43:04:47	9	28	d109	strong nebulosity; Rad:IRAS 16524-4300, Rad:GBM2006] 16524-4300A; Mas:[SRM89] 16524-4300
VVV CL094	17:07:54	-40:31:38.6	20	20	d074	nebulosity, embedded; Rad:GPSR 346.077-0.055; IRAS 17043-4027
VVV CL095	17:10:55	-39:41:49	52	30	d074	no nebulosity; overdensity; Dark Cloud SDC G347.082-0.011
VVV CL096	17:11:41	-41:19:03	10	17	d036	weak nebulosity, embedded; faint
VVV CL097	17:11:46	-41:18:13	10	20	d036	weak nebulosity, embedded; faint; IR:IRAS 17082-4114

Table 1. continued.

Name	RA(J2000) hh:mm:ss	DEC(J2000) deg:mm:ss	Numb.	Radius arcsec	Tile	Comments
VVV CL098	17:13:06	-38:59:45	13	20	d113	nebularity:IRAS 17096-3856; IR:MSX5C G347.9026+00.0486; Rad:GPSR 347.901+0.048; Mas:Caswell CH3OH 347.90+00.05
VVV CL099	17:14:26	-38:09:51	52	30	d114	no nebularity; X:CXOU J171424.4-380959
VVV CL100	17:19:15	-39:04:34	22	20	d075	nebularity:IRAS 17158-3901; Mas, Rad:GBM2006] 17158-3901; stellar group

Appendix A: Three-Color JHK_S Composite Images of the Cluster Candidates.







C1095



C1096



C1097



C1098



C1099



C1100